Proton transfer to charged platinum electrodes. A molecular dynamics trajectory study

2010 J. Phys.: Condens. Matter 22 175001

(http://iopscience.iop.org/0953-8984/22/17/175001)

IOP Publishing Journal of Physics: Condensed Matter

J. Phys.: Condens. Matter **22** (2010) 175001 (13pp) doi:10.1088/0953-8984/22/17/175001

Proton transfer to charged platinum electrodes. A molecular dynamics trajectory study

Florian Wilhelm[1,3], **Wolfgang Schmickler**[1] **and Eckhard Spohr**[2,4]

[1] Institute of Theoretical Chemistry, Ulm University, D-89069 Ulm, Germany
[2] Lehrstuhl für Theoretische Chemie, Universität Duisburg-Essen, D-45141 Essen, Germany

E-mail: eckhard.spohr@uni-due.de

Received 26 November 2009, in final form 5 February 2010
Published 23 March 2010
Online at stacks.iop.org/JPhysCM/22/175001

Abstract

A recently developed empirical valence bond (EVB) model for proton transfer on Pt(111) electrodes (Wilhelm *et al* 2008 *J. Phys. Chem.* C **112** 10814) has been applied in molecular dynamics (MD) simulations of a water film in contact with a charged Pt surface. A total of seven negative surface charge densities σ between -7.5 and -18.9 μC cm^{-2} were investigated. For each value of σ, between 30 and 84 initial conditions of a solvated proton within a water slab were sampled, and the trajectories were integrated until discharge of a proton occurred on the charged surfaces. We have calculated the mean rates for discharge and for adsorption of solvated protons within the adsorbed water layer in contact with the metal electrode as a function of surface charge density. For the less negative values of σ we observe a Tafel-like exponential increase of discharge rate with decreasing σ. At the more negative values this exponential increase levels off and the discharge process is apparently transport limited. Mechanistically, the Tafel regime corresponds to a stepwise proton transfer: first, a proton is transferred from the bulk into the contact water layer, which is followed by transfer of a proton to the charged surface and concomitant discharge. At the more negative surface charge densities the proton transfer into the contact water layer and the transfer of another proton to the surface and its discharge occur almost simultaneously.

(Some figures in this article are in colour only in the electronic version)

1. Introduction

Proton transfer to a metal electrode is a fundamental process in electrochemistry which, after decades of research, is still poorly understood. A proton can only exist in aqueous media as part of a solvated charged complex such as the Eigen complex $H_9O_4^+$ (a solvated hydronium H_3O^+ ion) [1] or the Zundel ion $H_5O_2^+$ [2], in which it is bound to several water molecules. In all aqueous systems the proton is not a well-defined species, since it is rapidly exchanged with the hydrogen atoms of the water molecules in processes which transform different complexes into each other. Distinguishing between the different complexes is thus experimentally demanding (see e.g. [3]), and evidence in favor of both the Eigen and the Zundel states of a proton in aqueous solution has been reported in the literature [4–7].

The basic idea of the so-called *Grotthuss hopping* mechanism for proton transfer in bulk water was established a long time ago [8]. State-of-the-art molecular dynamics techniques, which were developed during the last decade [9–19], have recently, together with other theoretical and experimental advances, contributed substantially to the detailed understanding of the nature of proton transfer processes. The rate-determining step of the reaction was identified as the breaking of a hydrogen bond in the solvation shell of the proton transferring cluster (*Moses mechanism* [20]). However, several questions still remain open in bulk water [12, 17, 18, 21–23], and even for advanced *ab initio* molecular dynamics simulation techniques substantial deviations from experimental values

[3] Present address: Zentrum für Sonnenergie- und Wasserstoff-Forschung (ZSW) Baden-Württemberg, D-89081 Ulm, Germany.
[4] Author to whom any correspondence should be addressed.

exist, in addition to problems related to the functionals and methods [12, 17, 24]. Available data and insight is, however, consistent with regarding Zundel and Eigen species as limiting forms [21] rather than separate species, and that the barrier for the proton transfer interconversion process between them is insignificantly small [13, 21].

In this situation it seems attractive to exploit *ab initio* molecular dynamics schemes also for the investigation of proton transfer to an electrode surface. However, as a quick estimate shows, this is currently not a realistic option. The heavy computational burden of such simulations allows at best the study of a few picoseconds of real time with an electrode area of one to two nanometer squared. Even on a good catalyst like platinum, transfer of a proton *to* the metal surface—as opposed to *within* the water layer, cf [25]—onto such a small area is highly improbable during such a short time. The few attempts that have been made in this direction (e.g. [26–28]) have therefore been performed at excessively high electric fields. Although the method employed appears promising for describing the electronic properties of the final reaction step, achieving a realistic characterization of the overall reaction dynamics comprising statistical averaging is still far from accomplishable.

Another approach to describe electrochemical reactions which has been extensively used during recent years [29–36] makes use of state-of-the-art density functional theory (DFT) techniques to obtain energy minimum structures at 0 K. These neglect the finite temperatures at which electrochemical reactions take place and do not explicitly treat the water molecules which are, as is shown in the bulk (see above), part of all proton complex interconversion processes. This treatment is based on the assumption that the water phase is not crucial for the rate-determining step of the reaction. In some works water is modeled in an ice-like, often bilayer structure. The latter results from geometry optimization and is comparable to corresponding low-temperature structures found in experiment [37]. Undoubtedly, for the chosen structure this method gives accurate results as far as the *potential* energy changes during electrochemical reactions are concerned, but neither electrode potential nor field are kept constant during the reaction. Nørskov and co-workers recently also showed that the potential difference at the protonated water/platinum(111) interface does not depend crucially on temperature, as can be inferred by the similarity of the potential difference across the room-temperature liquid–solid interface (simulated for a few ps) and across the surface at 0 K, provided that no less than three water layers are used in the study [38]. However, when it comes to the modeling of reaction rates, the solvent dynamics has to be addressed to describe hydrogen bond breaking and forming processes associated with water reorientation and diffusion in a comprehensive way.

Recently, a theory for the electrocatalysis of the hydrogen reaction has been proposed, which combines elements of Marcus theory [39], the Anderson–Newns model [40, 41] and DFT calculations. It focuses on the effect which the electronic structure of the electrode has on the reaction rate, and seems to explain reaction trends quite well [42]. However, while solvent effects are an essential part of this model, they are combined in a single parameter, the solvent reorganization energy familiar from Marcus theory. Naturally, this gives no information about interesting details like the breakup of the Zundel or Eigen ions.

Classical molecular dynamics simulations, based on model potentials, are computationally less demanding than the aforementioned methods and thus allow the study of larger systems over significantly longer time spans. However, the force fields commonly used in these simulations cannot describe the breaking of bonds, and are therefore also unsuitable for the investigation of electrochemical proton transfer, in which the breaking of hydrogen bonds must play a crucial role. One way to overcome the shortcomings of classical molecular dynamics are reactive force fields. In particular, the empirical valence bond (EVB) method, which is based on the ideas of Pauling and Coulson [43], has recently been developed into a viable scheme to describe the proton transfer reaction. The EVB method was pioneered by Warshel, e.g. [44–46], and later adopted for proton transfer in water, e.g. [47–49]. Further development of the method towards a multi-state description [14–16, 19, 21] has aided the construction of sophisticated models of proton transfer [13, 17, 18] and led to deeper insight into the details of the mechanism of proton transfer [23].

EVB schemes allow, due to their relative simplicity, simulations over a much longer timescale than *ab initio* methods, and are therefore attractive for the simulation of electrochemical proton transfer, at least when the driving force of the reaction is large. Existing implementations to date have been mostly designed to work for homogeneous transfer. We have therefore adapted the EVB method to the electrochemical inhomogeneous situation. To do this, the most challenging task lies in establishing the most important terms that couple the proton to the metal surface and describing this behavior in a simple fashion. For the Pt(111) electrode, which we have chosen as a first example, we have determined these terms by quantum chemical methods.

The model was described in detail in a previous communication [50] (termed EVB1 below). Here we will only briefly repeat the most important aspects from EVB1 in the next section. We then investigate some general characteristics of the hydrogen discharge reaction by analyzing individual trajectories. The proton discharge kinetics is analyzed using the distribution of transfer times and mean reaction rates. Energetics of the proton transfer complex, average trajectories, and orientational distributions of water molecules are then discussed to establish mechanistic trends as a function of surface charge density σ, which is followed by some general conclusions concerning the reaction mechanism of the Tafel step of the hydrogen evolution reaction.

2. Models and simulations

We will briefly review the major features of our empirical valence bond (EVB) simulation model which was discussed in detail in EVB1, where all details concerning the design and parameters of the model can be found. EVB models were developed first by Warshel and co-workers [44–46] in analogy to the valence bond approach in electronic structure theory,

where the electronic ground state ψ is described as a resonance hybrid, which is a superposition (or linear combination with coefficients c_i) of several resonance structures $|i\rangle$ as

$$|\psi\rangle = \sum_i c_i |i\rangle. \quad (1)$$

In an empirical valence bond model each basis state $|i\rangle$ corresponds, for the same set of atomic coordinates, to a specific arrangement of chemical bonds in a classical force field description of the entire system, i.e. $H_{ii} = \langle i|\hat{H}|i\rangle$ is the energy of a classical force field for a specific bond pattern. In general, each of these bond patterns corresponds to a significantly different energy both due to interactions within the system and due to interactions with the environment. The force fields and their parameters are chosen in order to describe the specific resonance structures of the system adequately. The off-diagonal elements $H_{ij} = \langle i|\hat{H}|j\rangle$ in an EVB model are often described by analytical functions fitted to either experimental information on barrier heights (e.g., in vacuo), or to the results of *ab initio* calculations for small systems. Applying this approach, the Hamiltonian is a function of the nuclear coordinates only, and the ground state can be obtained by solving an eigenvalue problem. By employing the Hellmann–Feynman theorem one can calculate all forces necessary for MD.

Here we use a 9-state EVB model describing both states featuring a proton bound to water molecules and states featuring a hydrogen atom bound to surface platinum atoms. Proton interaction with water molecules is based on a polarizable two-state EVB model developed for bulk liquid water by Walbran and Kornyshev [51]. Within our model, the proton charge in these two EVB states is compensated by a negative charge on the metal slab distributed evenly to the lowest layer of the 4-layer Pt(111) slab. Additionally, the model describes binding of the (discharged) hydrogen atom with the platinum surface by incorporating seven extra states involving a metal–hydrogen bond. These involve the Pt atom closest to the candidate H atom for proton transfer and its six nearest neighbors on the Pt(111) surface. In summary, the employed EVB model is able to describe bond breaking and formation together with charge transfer to the surface.

When the proton complex is far from the surface, its behavior is approximately reproduced as an interchange of the limiting species within the Walbran model [51], an hydronium ion H_3O^+ and a Zundel ion $H_5O_2^+$. Couplings between the proton complex and the metal surface are zero and the discharged states to do not contribute to the ground state. Grotthuss proton hops from one water molecule to another one are possible, i.e., the composition of the EVB cluster can change with time. Close to the surface, coupling with the metal states sets in and proton transfer is possible both between water molecules and between water and metal atoms, accompanied by discharge in the latter case. Many more details about the procedure, the criteria and the methods to obtain the model parameters are given in EVB1.

The electrode potential cannot be specified directly within a canonical (constant NVT) MD simulation, whereas specification of the surface charge (density) is straightforward. For a recent discussion of techniques to handle electrode potentials in DFT based electronic structure calculations, the reader is referred to the recent work by Nørskov *et al* [38] and the references cited therein. In order to investigate the influence of electrode potential on the proton transfer reaction in an indirect manner, we have chosen to perform MD simulations of solvated protons for seven negative platinum surface charge densities σ, ranging between -7.5 and -18.8 μC cm^{-2}. There is an ongoing debate in the literature about the exact position of the potential of zero charge of Pt(111), but a value of 0.4 V versus the reversible hydrogen electrode (RHE) provides a reasonable approximation [52]. Likewise, the double layer capacity is not certain, since it is difficult to separate double layer charging from adsorption [53]. Since the value for slow charging, which is of relevance here, is approximately 30 μF cm^{-2}, surface charge densities of -7.5 and -18.8 μC cm^{-2} correspond to electrode potentials of approximately 0.15 and -0.2 V relative to the RHE.

The simulated system consists of a (rigid) platinum slab (with (111) surface geometry; 256 atoms in 4 layers) onto which a film of 256 water molecules and the $H_5O_2^+$ entity was deposited. The simulation cell is a tetragonal box of $22.2 \times 19.23 \times 80.00$ Å^3. The length of the box in the z-direction leads to a large vacuum region between the water layer and the next periodic image in order to keep artificial interactions between the periodic images small. Coulomb interactions were calculated using the Ewald summation method in three dimensions. A mean temperature of 298.15 K was maintained with a Berendsen [54] thermostat (time constant 2.5 ps) for temperature control. The equations of motion were integrated using the velocity Verlet algorithm with a time step of 0.25 fs.

For each surface charge density, at least 30 trajectories were integrated, starting from independent configurations of an equilibrium trajectory. The equilibrium trajectory was started by placing the proton transfer cluster $H_5O_2^+$ into the aqueous film more than 12 Å from the surface and the EVB switching algorithm was turned off. Thus, the $H_5O_2^+$ complex corresponds to a pure diabatic state of a H_3O^+ ion and a close-by water molecule. In order to prevent this constrained $H_5O_2^+$ complex from rapidly approaching the negatively charged surfaces, in particular at high surface charges, it was confined by a repulsive umbrella potential to the region beyond 12 Å from the surface. Initial configurations for the trajectories were extracted at time intervals of 3 ps.

Subsequently, trajectories were started by turning off the confining potential and turning on the EVB switching algorithm. The zero of time for the trajectory was defined as the point when the hydronium barycenter came closer than 10 Å to the surface. Although the trajectory was originally started from a pure EVB ($H_3O^+ + H_2O$) state, at the thus-defined zero of time the $H_5O_2^+$ complex had evolved to some (unspecified) hydronium–Zundel superposition state. Trajectories were integrated until 2.5 ps after the proton was transferred to the metal slab. Depending on surface charge density, the total length of trajectories (i.e. including the steps before time measurement was started) varied between about 10 ps and approximately 600 ps.

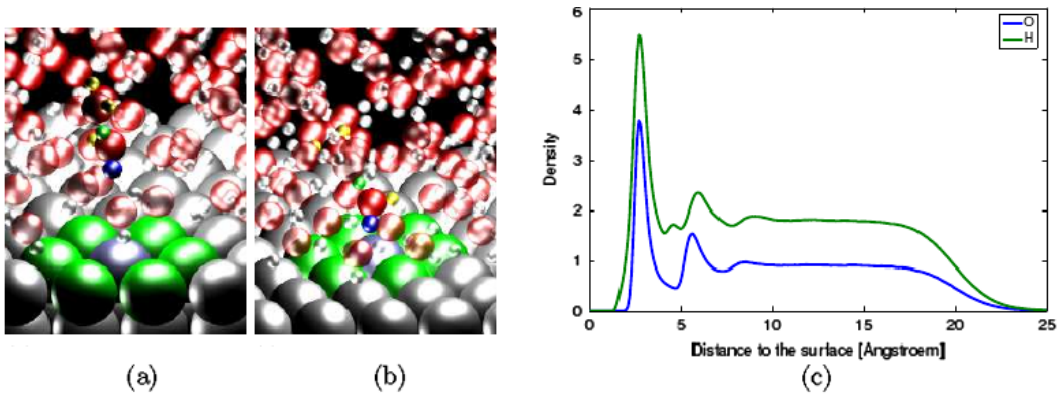

Figure 1. (a) Snapshot of an adsorbed $H_5O_2^+$ complex; (b) snapshot of proton transfer to the surface; (c) oxygen and hydrogen atom density profiles at $\sigma = -7.5\ \mu C\ cm^{-2}$.

Figure 1 shows two snapshots of the system at a surface charge density of $\sigma = -7.5\ \mu C\ cm^{-2}$, one of an adsorbed $H_5O_2^+$ ion (a) and one of a proton transfer event (b) together with the simulation averaged oxygen and hydrogen atom density profiles (c). The density profiles are similar to the ones published before using the same water–metal interactions [55]. Both atom profiles are consistent with a rapidly decaying layering of water molecules into a well-defined first layer (maximum in the oxygen profile at ≈2.6 Å), a diffuse second layer (maximum at ≈5.5 Å) and traces of a third water layer (≈8 Å). The hydrogen density profile shows an intermediate maximum at around ≈4.5 Å, which is characteristic for the hydrogen bonding taking place between the first two layers. Starting at around 17 Å, the film density smoothly decays to 0 at the liquid/vacuum interface.

3. Results

3.1. Individual trajectories

In EVB1 we briefly discussed mechanistic aspects on the basis of a few individual trajectories. Here, this discussion will be intensified and substantially extended, based on a statistically relevant number of trajectories. At low negative surface charge densities, we frequently observed adsorption of the fluctuating Zundel complex on the metal surface, with discharge and proton transfer to the metal surface occurring at a much later time, indicating that adsorption and discharge are separate processes. At larger negative surface charge densities, an adsorbed state of the Zundel complex is not discernible and discharge of the proton complex can occur almost simultaneously with the last proton hopping step into the first water layer facing the surface. The number of metal EVB states involved in the discharge process is also observed to vary significantly. Some trajectories involve essentially one metal state (indicating on-top adsorption of the discharged hydrogen atom) while others involve several metal EVB states, indicating a higher mobility of the hydrogen atom on the platinum surface and adsorption on hollow or bridge sites.

The overall variability of the time needed for discharge is quite large, which is not surprising considering the fact that several water molecules with substantial conformational freedom participate in the process. In order to quantify the proton discharge kinetics, we have measured the time for discharge in our trajectories as the time interval between an initial Zundel ion state and a final adsorbed hydrogen state. The initial Zundel ion state (or the zero of time, t_0) is defined when the barycenter of the $H_5O_2^+$ complex is closer than 10 Å to the metal surface for the first time during the trajectory (see also above). The final hydrogen adsorption state is defined as a configuration in which the sum of the weights of the seven metal EVB states exceeds 90% of the total weight, i.e., the charge on the $H_5O_2^+$ complex is less than $0.1e$. The discharge time t_D is defined as the difference between t_0 and the time when the final hydrogen adsorption state is reached for the first time, t_f. In addition, we defined an intermediate $H_5O_2^+$ adsorption state as a configuration in the trajectory when both the 'candidate' for discharge among the hydrogen atoms and the oxygen atom it is bound to are located in the first water layer ($z < 4.5$ Å, see figure 1). Based on this definition, the time for adsorption-to-discharge t_{AD} is defined as the difference between the point on the trajectory when the adsorption state is *reached for the last time* before proton transfer and t_f. Finally, a time for bulk-to-adsorption t_{BA} can be defined as

$$t_{BA} := t_D - t_{AD}. \tag{2}$$

Figure 2 shows the distribution of the time needed for discharge in the—at least—30 trajectories for several metal surface charge densities as indicated. Quite expectedly, times become shorter with increasingly negative surface charge densities. It is obvious, on the other hand, that for all surface charge densities one or several trajectories with extraordinary long discharge times exist. Due to the limited number of trajectories we can only speculate here that the reason for these trajectories to remain non-reactive for such a long time is due to (yet unknown) specific local structural features of the adsorbed water layer. We expect that these trajectories will become reactive at some later time, either due to changes or relaxation of the local structure, or due to surface diffusion to another region with locally different structure. In the rate averages (see below) these few trajectories possess only little weight.

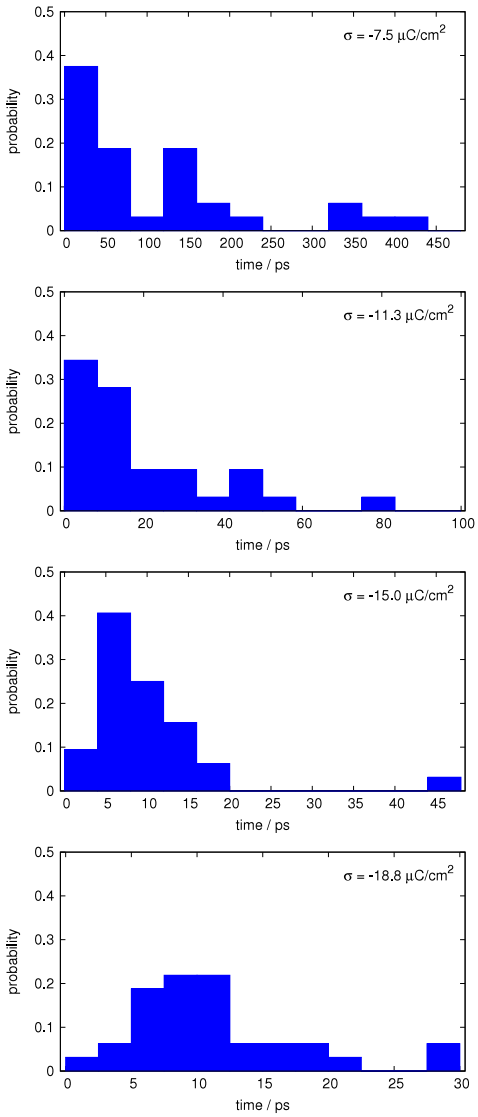

Figure 2. Histogram of total transfer times for trajectories at different surface charge densities as indicated. Note the vastly different timescale on the abscissas.

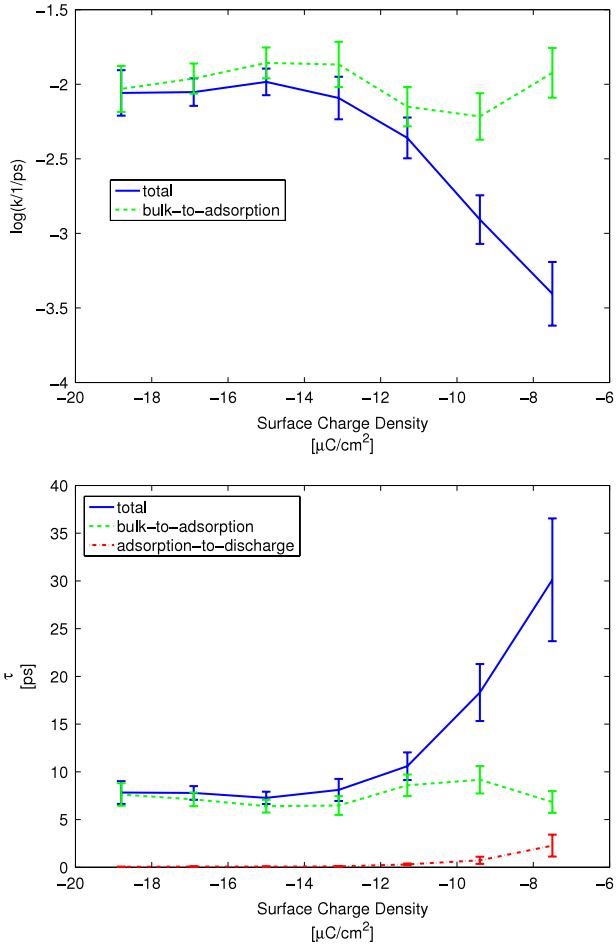

Figure 3. Rate constants. Top: logarithmic representation of the rate for discharge $\langle k_D \rangle$ (blue, full line) and the bulk-to-adsorption rate $\langle k_{BA} \rangle$ (green, dashed). Bottom: mean times for discharge $\langle \tau_D \rangle$ (blue, full line), bulk-to-adsorption time $\langle \tau_{BA} \rangle$ (green, dashed) and adsorption-to-discharge time $\langle \tau_{AD} \rangle$ (red, dash-dotted), see text for details and averaging method.

3.2. Proton discharge kinetics

We have calculated the mean rate constant for proton discharge, $\langle k_D \rangle$, and for bulk-to-adsorption, $\langle k_{BA} \rangle$, as the average over the reciprocal discharge and bulk-to-adsorption times, respectively, according to

$$\langle k_\alpha \rangle = \langle 1/t_\alpha(i) \rangle = \frac{1}{N} \sum_{i=1}^{N} t_\alpha^{-1}(i) \tag{3}$$

where i denotes trajectories and α can be either D or BA. Error bars are plotted as $\pm\sigma$ with the root mean square deviation σ of the average calculated as

$$\sigma = \sqrt{\frac{\langle k_\alpha^2 \rangle - \langle k_\alpha \rangle^2}{N-1}}. \tag{4}$$

Mean times $\langle \tau_\alpha \rangle$ were calculated as $\langle \tau_\alpha \rangle = 1/\langle k_\alpha \rangle$ with error bars obtained by Gaussian error propagation. By averaging the rates rather than the reaction times we avoid the practical problem that a reaction time would need to be defined 'ad hoc' for non-reactive trajectories, which can occur because the maximum simulation time necessarily has to be set to a reasonably short value.

It should be mentioned that for the higher negative surface charge values, the adsorption-to-discharge t_{AD} times were in some trajectories so short that they fell below the resolution of our monitoring of trajectory data, which was sampled in 25 fs intervals. In such cases, t_{AD} was set to 25 fs prior to calculating $\langle k_{AD} \rangle$.

The top part of figure 3 shows $\ln\langle k_\alpha \rangle$ as a function of the surface charge density σ for the total discharge rate (blue full line) and for the bulk-to-adsorption rate (green dashed line). $\ln\langle k_D \rangle$ increases approximately linearly with σ between -7.5 and -13.4 μC cm^{-2}, and reaches an almost constant plateau value for $\sigma < -13.4$ μC cm^{-2}. The value of $\langle k_{BA} \rangle$ is almost constant within the error limits.

The results indicate that at strongly negative surface charges the proton transfer reaction is dominated by the time the proton needs to approach the surface. At these surface

charge densities the process can be considered to be transport limited, although strictly speaking the motion of the single proton complex is migratory in the electric field produced by the surface charges and not diffusive. Furthermore, proton motion is of course not diffusive in the classical sense.

Once the proton complex reaches the surface at highly negative σ, proton transfer is almost immediate and, consequently, the time spent in the first water layer is very short. At less negative surface charge densities, the time the $H_5O_2^+$ complex spends in the adsorbed layer becomes more important and can be expected to dominate at even more positive surface charges (which are difficult to study within the present framework due to the excessively long simulation times necessary).

The bottom part of figure 3 shows the mean times $\langle\tau_\alpha\rangle$ for the total discharge time (blue full line) $\langle\tau_D\rangle$, the bulk-to-adsorption time $\langle\tau_{BA}\rangle$ (green dashed line) and for the adsorption-to-discharge time $\langle\tau_{AD}\rangle$ spent in the adsorbed first water layer (red dash-dotted line). Due to the rather small number of trajectories the error bars are substantial, but the major trends can clearly be extracted. (Note the somewhat smaller error bars for $\sigma = -16.9\ \mu C\,cm^{-2}$, where a total of 84 trajectories were calculated.)

The total mean time until discharge decreases rapidly from about 30 ps at $\sigma = -7.5\ \mu C\,cm^{-2}$ to values of about 10 ps at $-11.3\ \mu C\,cm^{-2}$. For even more negative values of σ the discharge times are roughly constant at around 7–8 ps. At these negative surface charge densities the reaction time is completely dominated by the time spent in the bulk during approach (green dashed curve). This time is practically constant within the limits of statistical errors. The time spent in the adsorbed state (red dash-dotted curve) is almost zero at these negative surface charge densities. At the more positive values it increases to a few picoseconds. One should note that by construction (we average over the rates, see equation (3)), the mean time spent in the bulk (4.5 Å $< z <$ 10 Å) and the mean time spent in the adsorbed state do not add up to the total time. This is very obvious at the more positive values of the surface charge density.

In summary, adsorption and proton transfer occur consecutively at more positive surface charge densities σ and occur almost simultaneously at negative values of σ.

3.3. Energetics

In order to investigate the overall energetics of the simulated proton discharge process, we extract the potential energy of the Zundel complex $H_5O_2^+$, E_{pot}. For this analysis and for further mechanistic investigations (see below), we separately analyze the data for each time step, starting 1000 time steps before the proton transfer event (defined as the first time during the trajectory at which the H-metal bond contribution to the adiabatic EVB state is more than 90%, see above) and ending 1000 time steps afterward. Thus, the data used below correspond to properties obtained over a time interval of 0.5 ps. The energy of the $H_5O_2^+$ complex was calculated as a function of two parameters $r_{O^*H^*}$ and $\cos\phi$, $E_{pot}(r_{O^*H^*}, \cos\phi)$ with

$$E_{pot}(r_{O^*H^*}, \cos\phi) = E_{intra,H_5O_2^+} + E_{H_5O_2^+-W} + E_{H_5O_2^+-metal} + E_{electrode} \quad (5)$$

averaged over all trajectories and all time steps during this 0.5 ps interval. $r_{O^*H^*}$ is the distance between the candidate atom H* (for proton transfer to the surface) to the oxygen atom O* to which it is bonded, and ϕ is the angle between the $\vec{r}_{O^*H^*}$ vector and the surface normal pointing into the aqueous region. $E_{intra,H_5O_2^+}$ is the intramolecular energy of the $H_5O_2^+$ complex, $E_{H_5O_2^+-W}$ the interaction energy between the $H_5O_2^+$ complex and all water molecules, $E_{H_5O_2^+-metal}$ the interaction energy between the $H_5O_2^+$ complex and all metal atoms and $E_{electrode}$ the interactions of all charges of the $H_5O_2^+$ complex with the charges modeling the electrode surface charge density. In practice E_{pot} is recalculated from the trajectories by taking the difference between the total potential energy and the potential energy of a system in which all atoms of the $H_5O_2^+$ complex are replaced by non-interacting ghost atoms. Figure 4 shows the trajectory and time average $\langle E_{pot}(r_{O^*H^*}, \cos\phi)\rangle$ for four different surface charge densities. Each point is averaged over all configurations and trajectories within a particular combination of $(\vec{r}_{O^*H^*}, \cos\phi)$ with $\delta r = 0.1$ Å and $\delta\cos\phi = 0.1$. Note that the number of configurations contributing to each average value may vary, depending on the course the trajectories take. Regions of $(\vec{r}_{O^*H^*}, \cos\phi)$ not visited by the trajectories are not shown. All energy values are given relative to the global minimum potential energy found in the analysis of all configurations in all trajectories at all surface charge densities studied.

The regions on the right side of the plots, i.e., $r_{O^*H^*} \approx 1$ Å and $\cos\phi > 0.5$ (close to the global energy minimum) correspond to the molecular bonding situation and orientation of a typical $H_5O_2^+$ complex, where the candidate hydrogen atom H* is bonded to the oxygen atom O* and the hydrogen atom points slightly away from the surface. H* is—by construction of the model—usually the hydrogen atom of the $H_5O_2^+$ complex closest to the surface. What cannot be seen from this figure, however, is the fact that configurations with $\cos\phi > 0.2$ are rather infrequent in the time interval immediately preceding and following proton transfer, and thus have a large statistical uncertainty.

The regions on the left side of the plots, i.e., $r_{O^*H^*} > 1.4$ Å and $\cos\phi < -0.5$ show the energy of the transferred species: the H*O* bond is broken and the now neutral hydrogen atom is adsorbed on the metal surface, so that $\vec{r}_{O^*H^*}$ points roughly towards the surface.

Between reactant and product regions there are large regions of configuration space never sampled by any of the trajectories. The connecting region is representative of the proton transfer step itself and overall is rather narrow, although its width increases somewhat with increasingly negative surface charge density. By comparing the mean energy in the reactant region to the mean energy in the product region, it is obvious that the proton energy increases at $\sigma = -7.5\ \mu C\,cm^{-2}$. Since the reaction nevertheless occurs rapidly, this implies that the increase in proton energy is counterbalanced by the solvent energy, which is not included in equation (5). Nevertheless, the question can be raised why there is no reverse reaction, leading from adsorbed hydrogen to dissolved $H_5O_2^+$ complexes. One reason is that all calculations have been stopped 2.5 ps after proton transfer, thereby making

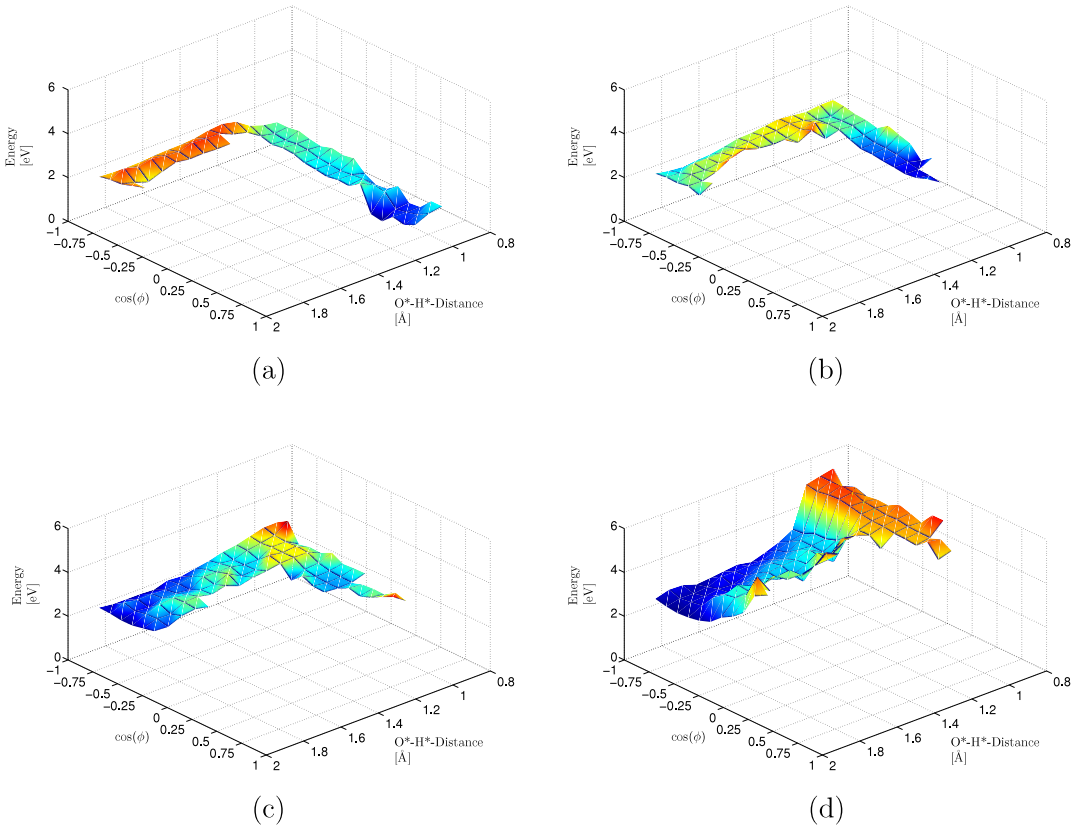

Figure 4. Mean potential energies $\langle E_{\mathrm{pot}} \rangle$ for proton transfer (for definition see text) at different charge densities σ as indicated. ϕ is the angle between the $\vec{r}_{\mathrm{O^*H^*}}$ vector and the surface normal. (a) $\sigma = -7.5\ \mu\mathrm{C\ cm^{-2}}$, (b) $\sigma = -9.4\ \mu\mathrm{C\ cm^{-2}}$, (c) $\sigma = -11.3\ \mu\mathrm{C\ cm^{-2}}$ and (d) $\sigma = -16.9\ \mu\mathrm{C\ cm^{-2}}$.

reverse reactions rather improbable as compared to the forward reaction. Furthermore, the two water molecules produced from the former $H_5O_2^+$ complex reorient and are incorporated into the hydrogen bond network of the aqueous environment shortly after proton transfer, which leads to orientationally and/or sterically unfavorable configurations for the reverse reaction. At any rate, investigating the back reaction was not within the scope of the present study.

Figures 4(b) and (c) shows that between $\sigma = -9.4$ and $-11.3\ \mu\mathrm{C\ cm^{-2}}$ reactant and product potential energies become rather similar with no statistically discernible barrier. Further decrease of σ to more negative values leads to an overall downhill energy profile for the proton discharge reaction (see figure 4(d) at $\sigma = -16.9\ \mu\mathrm{C\ cm^{-2}}$).

Figure 5 shows the evolution of the potential energy E_{pot} along seven arbitrarily chosen trajectories for two different values of σ in the $(r_{\mathrm{O^*H^*}}, \cos\phi)$ plane. It is apparent for $\sigma = -9.4\ \mu\mathrm{C\ cm^{-2}}$ (left) that trajectories evolve first towards increasing alignment antiparallel to the surface normal ($\cos\phi \rightarrow -1$), and only then does dissociation occur ($\vec{r}_{\mathrm{O^*H^*}}$ increases). At the more negative value $\sigma = -16.9\ \mu\mathrm{C\ cm^{-2}}$ the accessible region of configuration space broadens substantially and trajectories become dissociative before complete alignment has taken place. Apparently, the reduction of the effective barrier for discharge with increasingly negative values of σ makes reactive events more feasible in which the proton is transferred at an angle of substantially less than 180° to the surface, which gives rise to a wider spread of trajectories in the $(\vec{r}_{\mathrm{O^*H^*}}, \cos\phi)$ plane. By this process, hydrogen atoms end up more frequently in hollow and bridge than in on-top positions (see discussion below) and possibly possess a higher lateral excess kinetic energy after reaction, which will only slowly be thermalized due to the smoothness of the potential energy surface of the adsorbed hydrogen atom on Pt(111).

The diminishing tendency to prealignment of the transferring proton along the surface normal is even more obvious in the representation of figure 6. The figure shows the time-resolved trajectory average $\cos\phi$, $\langle\cos\phi\rangle(t)$. The time axes of all trajectories for a given surface charge density have been aligned such that the time of transfer as defined above is at $t = 0$. The time interval from 250 fs before and after the reaction is shown. At the lowest surface charge density of $\sigma = -7.5\ \mu\mathrm{C\ cm^{-2}}$ one clearly sees that $\langle\cos\phi\rangle$ starts to change from a value of around -0.3 (which indicates rather weak alignment) to values $\leqslant -0.9$ (which indicates almost complete alignment). This prealignment process already starts approximately 200 fs before the reaction. At the next lower surface charge densities ($\sigma = -9.4$ and $-11.3\ \mu\mathrm{C\ cm^{-2}}$) the alignment process starts approximately 70 and 50 fs before the proton transfer event. For the simulations at large negative surface charge density (-13.1 to $-18.8\ \mu\mathrm{C\ cm^{-2}}$), alignment and proton transfer occur almost simultaneously (within a 20 fs time interval). At positive times $\vec{r}_{\mathrm{O^*H^*}}$ remains aligned at $\sigma = -7.5\ \mu\mathrm{C\ cm^{-2}}$. This indicates on-top adsorption of the hydrogen atom, since the oxygen atom O* generally

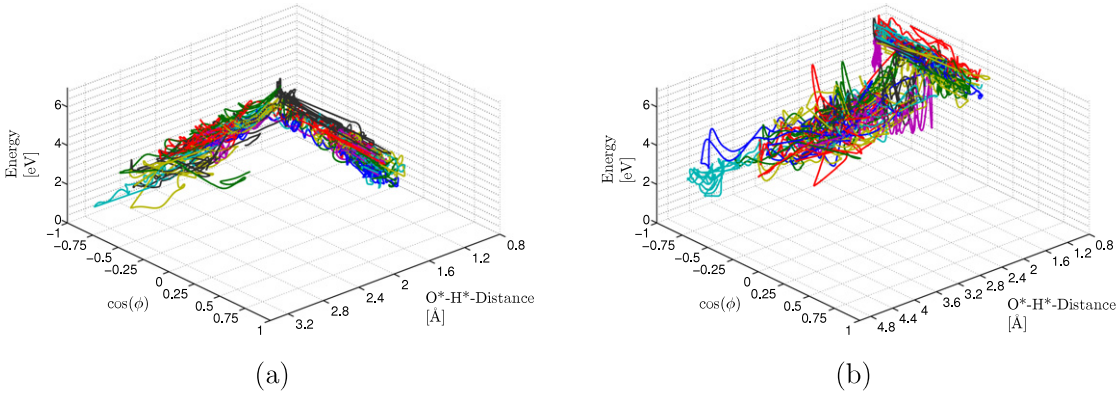

Figure 5. Potential energy E_{pot} along seven trajectories for (a) $\sigma = -9.4$ and (b) -16.9 μC cm^{-2}.

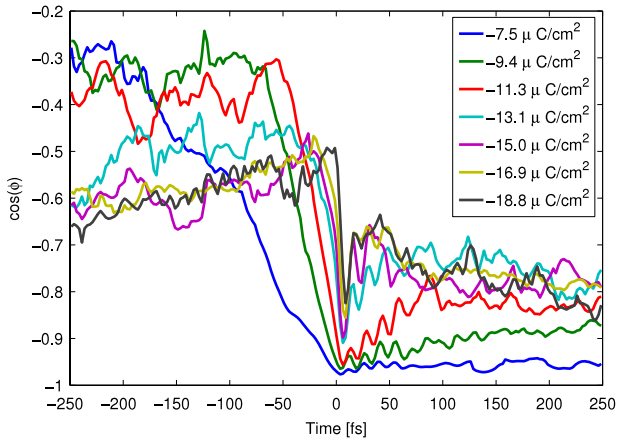

Figure 6. Trajectory averaged value of $\cos\phi$ for different surface charge densities. ϕ is the angle between the surface normal pointing into the aqueous region and the vector $\vec{r}_{\mathrm{O^*H^*}}$ between the discharging hydrogen atom and the oxygen atom to which it is bonded.

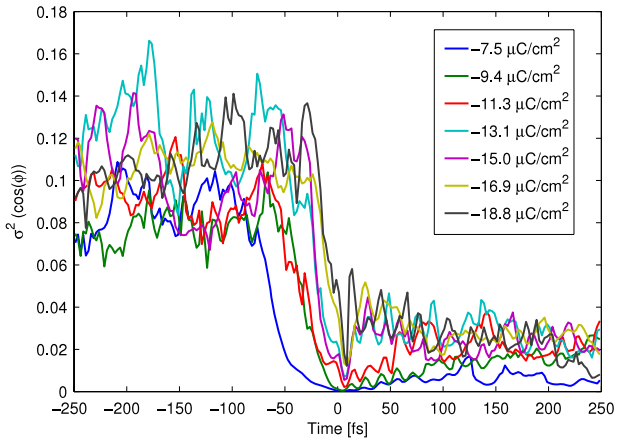

Figure 7. Variances $\sigma^2(\cos\phi) = \langle(\cos\phi)^2\rangle - \langle\cos\phi\rangle^2$ for different surface charge densities. ϕ is the angle between the surface normal pointing into the aqueous region and the vector $\vec{r}_{\mathrm{O^*H^*}}$ between the discharging hydrogen atom and the oxygen atom to which it is bonded.

should not move far from its initial position close to the on-top site of the platinum surface within the timescale taken into account here. With increasingly negative surface charge density this alignment decreases, which can be traced to an increasing population of hollow and bridge sites by the discharged hydrogen atom.

The variances of $\cos(\alpha)$, $\sigma^2(\cos\alpha) = \langle(\cos\alpha)^2\rangle - \langle\cos\alpha\rangle^2$ in figure 7 support this view. For the smaller charge densities the variances start decreasing to zero well before the reaction takes place, e.g. about 100 fs prior to reaction for $\sigma = -7.5$ μC cm^{-2}. A relatively small value of $\sigma^2 \approx 0.1$ is found for all charge densities prior to about -100 fs, which indicates incomplete yet significant alignment of $\vec{r}_{\mathrm{O^*H^*}}$, even at the larger surface charge densities.

3.4. Mechanistic trends

Time-resolved averaging of properties over all trajectories, similar to figure 6, can also be used to gain a deeper understanding of systematic trends in the shift of the nature of the proton state during the discharge process. Figure 8 shows averaged values of some squared EVB coefficients, which can be interpreted as weights of the diabatic states, see equation (1), as a function of time for several values of the surface charge density σ. Again, all time axes are shifted such that the proton transfer event is at $t = 0$. As described above and in detail in EVB1, the adiabatic EVB state of the proton complex is made up by the two 'water' states $|1\rangle$ and $|2\rangle$ and 7 'metal' states $|3\rangle$ to $|9\rangle$. State $|2\rangle$ is by construction the diabatic state which features the candidate hydrogen atom H* for proton transfer to the surface (see section 2) as part of the model hydronium ion. It can be regarded as the 'stepping stone' for proton transfer from the $H_5O_2^+$ complex to the surface.

Frames 8(a)–(e) show the time evolution of states $|1\rangle$ and $|2\rangle$ for different surface charge densities. Most interesting is the behavior shortly before transfer. At the charge density of $\sigma = -7.5$ μC cm^{-2} it is evident that, starting at about 100 fs, state $|2\rangle$ begins to dominate. Thus, during this time span the adiabatic state is dominated by the stepping stone state $|2\rangle$, i.e. a hydronium (or hydronium-like) state in the adsorbed water layer. At the more negative surface charge density of $\sigma = -11.3$ μC cm^{-2} this prevalence is very strongly reduced

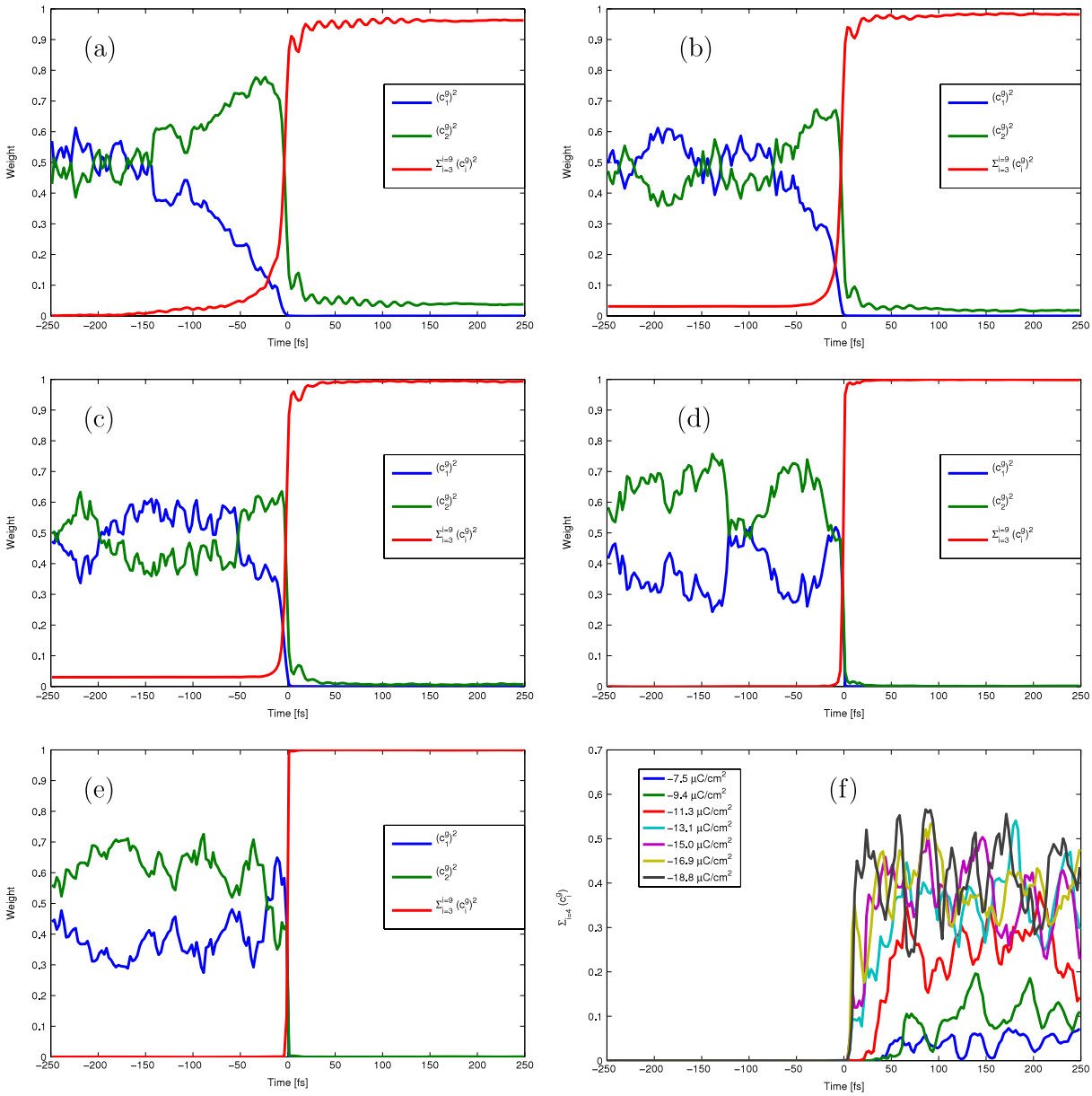

Figure 8. Trajectory averaged contributions of the diabatic states in the EVB complex. c_2^2 is the contribution of the H_3O^+ state at oxygen atom O* (usually in the first water layer), from which one hydrogen atom is dissociated during the discharge reaction, c_1^2 is the contribution of the H_3O^+ state at the other oxygen atom of the formal Zundel ion. In addition, the sum of all metal states $\sum_{i=3}^{9} c_i^2$ is shown in red. Data sets (a) through (e) contain results from simulations at −7.5, −9.4, −11.4, −15.0 and −18.8 μC cm^{-2}, respectively. Data set (f) contains the accumulated weight of metal states $|4\rangle$ through $|9\rangle$ for several different surface charge density values.

(and lasts less than 50 fs), and at even more negative charge densities it is absent altogether.

These results allow us to draw the following picture for proton transfer to the platinum surface: for low negative surface charge densities the process takes a stepwise course, i.e. after several (Grotthuss style) proton 'hops' through the bulk solution, the proton transfer cluster reaches the first water layer adsorbed on the metal surface and remains adsorbed for some time. Fluctuations eventually establish a situation where the O*–H* bond begins to point towards the surface and the 'bridging' hydrogen bond to the other oxygen atom within the Zundel complex is weakened. This leads to a hydronium-like, stepping stone state in the adsorbate layer with the H* atom being part of this hydronium ion. Finally, the proton is discharged and transferred to the surface.

In contrast, for very negative surface charge values, there is almost no latency between adsorption of the hydronium part of the proton cluster on the surface and discharge. Here the last Grotthuss step occurs almost simultaneously with the breaking of the O*H* bond, as can be inferred from the fact that the discharge step is preceded by a near-symmetrical $H_5O_2^+$ complex (states $|1\rangle$ and $|2\rangle$ have similar weights).

Another trend visible from figure 8 is the fact that with increasingly negative surface charge density the rise of the metal contributions (and thus the process of proton discharge) becomes increasingly faster. For the low surface charge

densities this process is not complete even 250 fs after the reaction event, as can be seen from the corresponding survival of the $|2\rangle$ contribution to the total state. At the more negative surface charge densities, proton discharge is complete within a few femtoseconds.

Figure 8(f) indicates another interesting fact. It shows the contribution of the non-pivot metal states $|4\rangle$–$|9\rangle$, i.e. those which do *not* correspond to H^* being bonded to the platinum atom (state $|3\rangle$) on top of which proton transfer takes place. This contribution is relatively small at $\sigma = -7.5\ \mu C\ cm^{-2}$ and then becomes successively larger with increasingly negative surface charge density. This indicates that for small σ the proton remains largely on top of the platinum atom to which the hydronium ion was bound, whereas at more negative σ the proton can also end up on the bridge and hollow positions. The increasing importance of bridge and hollow positions for the final proton position can be rationalized by two observations. In the discussion of figures 5 and 6 we noted that with increasingly negative σ the O^*–H^* vector needs to be less aligned, i.e., proton transfer can occur at smaller angles than 180° relative to the outward surface normal. On the other hand, the driving force for the reaction increases in the same direction, which leads to a larger excess kinetic energy of the proton, which manifests itself, e.g., in figure 8 and which most likely will (at least partially) be transformed into lateral kinetic energy. Combining these two effects leads to an increased weight of bridge and hollow positions, which in turn increases the contributions of states $|4\rangle$ through $|9\rangle$ to the overall hydrogen state. One should note here that our model has been designed [50] to reproduce the shallow barriers for hydrogen diffusion on the Pt(111) surface in vacuum as reported in the literature [56, 57]. Thus, after complete proton transfer and discharge, the water molecules surrounding the adsorbed hydrogen atom do not exert a large influence on the hydrogen species. Consequently, our model leads to similarly effortless surface diffusion of hydrogen near the water/metal interface as on the free metal surface. Recent DFT calculations by the group of Groß also show that the presence of water has indeed little influence on the mobility of adsorbed hydrogen atoms [58].

3.5. Orientational distribution

In order to round off our picture of proton transfer, we finally should direct some attention to the stand-alone behavior of the electrochemical surrounding of the reactants, i.e. the water layer facing the metal surface, with increasingly negative surface charge density. To gain insight into this issue, we have performed MD trajectories in the absence of the additional proton, i.e. just for the 'classical' system water–metal. Apart from that the relevant technical parameters were chosen, as in the reactive trajectory runs described above, to ensure comparableness. The variable of interest at this point is the statistical, molecule and trajectory averaged orientational behavior of the—for proton transfer to the surface—most relevant water molecules, those belonging to the first peak of the oxygen density distribution shown in figure 1.

Figure 9 shows the orientational distribution functions depending on two variables. $\cos(\alpha)$ is the angle between water dipole vectors and the surface normal (directed into the liquid phase), $\cos(\beta)$ is the corresponding angle between the proton–proton vector of water molecules and the same surface normal. Due to the symmetry of the water molecule, distributions were symmetrized with respect to $\cos(\beta)$. Figures 9(a) and (b) show the orientational distribution for the entire adsorbate layer (oxygen z coordinates between 0 and 4.5 Å, cf figure 1) at $\sigma = -7.5$ and $-18.8\ \mu C\ cm^{-2}$.

At $\sigma = -7.5\ \mu C\ cm^{-2}$, two characteristic configurations of water molecules are discernible: a pronounced maximum around $\cos(\alpha) \approx \cos(\beta) \approx 0$ represents water molecules which lie mostly flat inside the adsorbed water layer (and usually form donative hydrogen bonds within this layer). Two other maxima at $\cos(\alpha) \approx 0.5$ and $\cos(\beta) = \pm 0.8$ characterize those water molecules which (predominantly) form one hydrogen bond within the adsorbate plane and another one towards the second layer. With increasingly negative surface charge density σ (figure 9(b)), the first maximum moves towards more negative values of $\cos(\alpha)$, indicating an increasing orientation of the water dipole towards the more negatively charged surface. The second maxima become less pronounced.

To understand these average features of the entire first layer, one can take a closer look at the two halves which make up the first oxygen density peak in figure 1. The water molecules which are situated closest to the metal surface (left half of the peak, oxygen z coordinate $z < 2.64$ Å), figures 9(c) and (d), show distinct differences with the surface charge density. At $\sigma = -7.5\ \mu C\ cm^{-2}$, the maximum at $\cos(\beta) \approx 0$ is more pronounced and shifts towards more positive values of $\cos(\alpha)$, while the second maximum is at a similar position. At $\sigma = -18.8\ \mu C\ cm^{-2}$, however, the distribution has changed and there is a substantial probability density for protons to point more strongly towards the surface ($(\cos\alpha, \cos\beta) \approx (-0.6, \pm 0.7)$). Consequently, we can expect that a Grotthuss step from a second layer H_3O^+ ion to one of these first layer water molecules is facilitated by the fact that the oxygen end of the water molecule points towards the second layer. Furthermore, when such a step occurs, both protons of the accepting water molecule are promising candidates for an almost instantaneous transfer to the surface, since no major water reorientation is necessary. The water molecules within the surface-adverted half of the first peak show a comparatively less explicit behavior, although the general trend to align the water dipole vector rather towards the surface can be seen from figures 9(e) and (f). These findings back our conclusions drawn from the proton transfer trajectories, as described in the previous sections.

4. Conclusion

Molecular dynamics trajectory calculations using empirical valence bond models form a suitable approach for the simulation of chemical reactivity involving many degrees of freedom, such as the first step of proton discharge on a metal electrode. Here we have simulated proton transfer

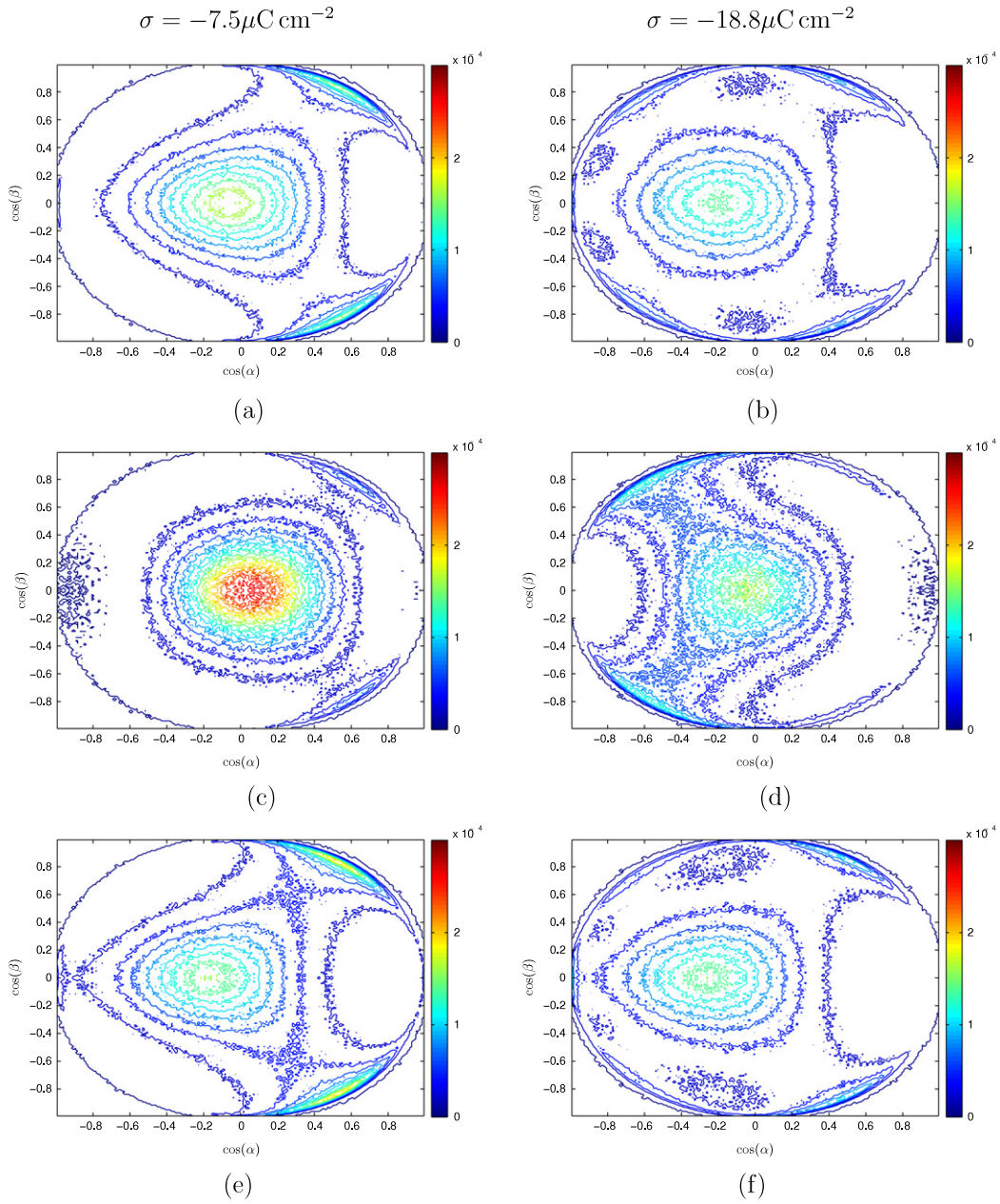

Figure 9. Two-dimensional histograms for the distribution of the angles of the water dipole vector α and the proton–proton vector β relative to the surface normal for different surface charge densities σ and different distance ranges from the surface. (a) First layer (0Å $< z <$ 4.5 Å), (b) first layer (0 Å $< z <$ 4.5 Å), (c) 0 Å $< z <$ 2.64 Å, (d) 0 Å $< z <$ 2.64 Å, (e) 2.64 Å $< z <$ 4.5 Å and (f) 2.64 Å $< z <$ 4.5 Å.

within a slab of liquid water in contact with a platinum slab for different values of surface charge density. The method is capable of performing multiple simulations of the electrochemical interface over time periods of the order of nanoseconds. This allows us to systematically study the proton transfer rate to the metal surface as a function of the electrochemical variable surface charge density. Simulations are started from equilibrated configurations where the proton complex is initially located in the liquid 'bulk' far from the surface, and then proceed until the discharge reaction occurs. This procedure, however, limits the accessible regime of surface charge densities to values sufficiently negative such that the discharge occurs within about 1 ns.

As has been stated above, the least negative surface charge density applied in the current investigation, $\sigma = -7.5\ \mu\mathrm{C\,cm^{-2}}$, corresponds to an electrode potential of ≈0.15 V versus the reversible hydrogen electrode (RHE). This is well within the range where adsorption of a full hydrogen layer is observed experimentally. This range begins approximately at the potential of zero charge, which is about 0.4 V more positive than actual hydrogen evolution at the RHE potential, which is at 0 V by definition. The experimental rate of underpotential deposition in this range is actually too fast to be measured. The observed onset of H discharge in our simulation falls into this range as well. For the chosen area of our simulation box, the exchange current density at

$-7.5\ \mu C\ cm^{-2}$ is of the order of 10^{10} A cm^{-2}. Accordingly, at the very least one can make the statement that there is no contradiction between known experimental data and the results of our simulation.

Reaction times in this electrochemical reaction for a given value of surface charge density σ vary quite substantially, at least at the lower-magnitude values of σ investigated here. This is a consequence of the many degrees of freedom which participate in the transfer of the proton from the bulk into the adsorbate layer, and then in the combined discharge and transfer to the metal surface. For the mean reaction rates we observe two different regimes of behavior. For moderately negatively charged metal surfaces in the regime $\sigma > -11.3\ \mu C\ cm^{-2}$, the reaction rate increases approximately exponentially with the surface charge density, in accordance with the expected Tafel behavior of this reaction. At more negative values of σ, the observed reaction rate is roughly constant, which indicates that in this range the reaction is transport limited. It should be noted that this transport involves a combination of diffusion and migration, since the 'free' proton in the aqueous solution migrates in the unscreened electric field generated by the charged surface—additional ions to screen the electrode potential are presently absent in our model. In fact, the simulations show that the mean rate to form an adsorbed Zundel ion (i.e. a complex which is located in the first water layer) is approximately independent of σ.

We can thus interpret our results in the following way. At high surface charge densities the rate-determining step of the discharge reaction is the approach of the proton complex via a combination of Grotthuss proton jumps and classical diffusion towards the surface. Proton discharge after adsorption is fast under these conditions. With increasingly less negative values of σ, the rate of adsorption does not change much, but the rate for establishing an orientational fluctuation of the Zundel complex suitable for proton transfer to the surface becomes smaller. Eventually, this step becomes rate determining.

At the highest surface charge densities the mechanism approaches a concerted two-proton transfer, where proton transfer from the second layer into the first layer occurs almost simultaneously with the transfer and discharge of a peripheral proton of the Zundel complex to the metal. At less negative values of σ, the mechanism becomes similar to the one proposed by Pecina and Schmickler [59, 60] for non-catalytic metals. They predict that reorientation of a water molecule taking place *within* the adsorbed layer preceding the concerted transfer step is rate determining. Here we find that reorientation of a water molecule in the adsorbed water layer is not rate determining at large negative surface charge densities, because proton transfer may occur even without strong orientational preference at these charge densities (see e.g. discussion of figures 4 and 6), and also because the surface charge induced mean water orientation with hydrogen atoms pointing towards the surface (see figure 9) becomes more suitable for direct proton transfer from the second layer. However, at low negative surface charge densities there is definitely a characteristic latency during which a proton complex *within* the adsorbed water layer has already formed but has not yet relaxed to the optimal orientation for proton discharge. Hence, at low negative surface charge densities, our model predicts a stepwise rather than a concerted process of adsorption and reorientation.

The EVB model based simulation approach, being inherently a classical MD approach, does not address quantum tunneling effects, which on the one hand might become important at high barrier heights, but which on the other hand may be neglected when the barrier is small (as is true for the case studied here) and washed out by zero-point motions (see, e.g. the results of *ab initio* path integral simulations in [11]). For the sake of simplicity, the EVB model employed is based on the minimum number of two water states—it thus can mimic Grotthuss jumps approximately as a series of $H_5O_2^+ \rightarrow H_3O^+ \rightarrow H_5O_2^+$ transitions—and a small number of 7 metal states; it could of course be extended to incorporate more water and more metal states. Especially the correctness of the mechanistic description of proton transfer within bulk water can be expected to remarkably benefit from such an extension. At the same time, the conceptual and computational complexity would necessarily increase, in conflict with the primary objectives of this work.

Finally, our simulation approach can also be employed to investigate the temperature dependence of proton discharge as well as its dependence on different electrode metals. Such applications will be reported in a future communication.

Acknowledgments

Financial support from the Deutsche Forschungsgemeinschaft (Schm 344/32) is gratefully acknowledged. The authors thank R R Nazmutdinov for many helpful discussions.

References

[1] Eigen M 1963 *Angew. Chem.* **75** 489–508
[2] Zundel G and Metzger H 1968 *Z. Phys. Chem. Neue Folge* **58** 225–45
[3] Brooker M H 1986 *The Chemical Physics of Solvation. Part B* ed R R Dogonadze, E Kálmán, A A Kornyshev and J Ulstrup (Amsterdam: Elsevier) pp 149–85
[4] Kobayashi C, Iwahashi K, Saito S and Ohmine I 1996 *J. Chem. Phys.* **105** 6358–66
[5] Heinzinger K and Weston R E 1964 *J. Phys. Chem.* **68** 744–51
[6] Conway B E 1981 *Ionic Hydration in Chemistry and Biophysics* (Amsterdam: Elsevier)
[7] Zundel G and Fritsch J 1986 *The Chemical Physics of Solvation. Part B* ed R R Dogonadze, E Kálmán, A A Kornyshev and J Ulstrup (Amsterdam: Elsevier) pp 21–96
[8] de Grotthuss C J T 1806 *Ann. Chim.* **58** 54–74
[9] Tuckerman M E, Laasonen K, Sprik M and Parrinello M 1995 *J. Chem. Phys.* **103** 150–61
[10] Tuckerman M E, Marx D, Klein M L and Parrinello M 1997 *Science* **275** 817–20
[11] Marx D, Tuckerman M E, Hutter J and Parrinello M 1999 *Nature* **397** 601–4
[12] Izvekov S and Voth G A 2005 *J. Chem. Phys.* **123** 044505
[13] Marx D 2006 *ChemPhysChem* **7** 1848–70
[14] Vuilleumier R and Borgis D 1999 *J. Chem. Phys.* **111** 4251–66
[15] Schmitt U W and Voth G A 1999 *J. Chem. Phys.* **111** 9361–81
[16] Brancato G and Tuckerman M E 2005 *J. Chem. Phys.* **122** 224507
[17] Voth G A 2006 *Acc. Chem. Res.* **39** 143–50

[18] Swanson J, Maupin C, Chen H, Petersen M, Xu J, Wu Y and Voth G 2007 *J. Phys. Chem.* B **111** 4300–14
[19] Wu Y, Chen H, Wang F, Paesani F and Voth G 2008 *J. Phys. Chem.* B **112** 467–82
[20] Agmon N 1995 *Chem. Phys. Lett.* **244** 456–62
[21] Day T J, Soudackov A V, Čuma M, Schmitt U W and Voth G A 2002 *J. Chem. Phys.* **117** 5839–49
[22] Kornyshev A A, Kuznetsov A M, Spohr E and Ulstrup J 2003 *J. Phys. Chem.* B **107** 3351–66
[23] Lapid H, Agmon N, Petersen M K and Voth G A 2005 *J. Chem. Phys.* **122** 014506
[24] VandeVondele J, Mohamed F, Krack M, Hutter J, Sprik M and Parrinello M 2005 *J. Chem. Phys.* **122** 014515
[25] Meng S 2005 *Surf. Sci.* **575** 300–6
[26] Sugino O, Hamada I, Otani M, Morikawa Y, Ikeshoji T and Okamoto Y 2007 *Surf. Sci.* **601** 5237–40
[27] Otani M, Hamada I, Sugino O, Morikawa Y, Okamoto Y and Ikeshoji T 2008 *J. Phys. Soc. Japan* **77** 024802
[28] Otani M, Hamada I, Sugino O, Morikawa Y, Okamotode Y and Ikeshojiae T 2008 *Phys. Chem. Chem. Phys.* **10** 3609–12
[29] Jacob T and Goddard W 2004 *J. Am. Chem. Soc.* **126** 9360–8
[30] Taylor C D, Wasileski S A, Filhol J-S and Neurock M 2006 *Phys. Rev.* B **73** 165402
[31] Filhol J-S and Neurock M 2006 *Angew. Chem. Int. Edn* **45** 402–6
[32] Hinnemann B, Moses P G, Bonde J, Jørgensen K P, Nielsen J H, Horch S, Chorkendorff I and Nørskov J K 2005 *J. Am. Chem. Soc.* **127** 5308–9
[33] Greeley J, Jaramillo T F, Bonde J, Chorkendorff I and Nørskov J K 2006 *Nat. Mater.* **5** 909–13
[34] Nørskov J K and Christensen C H 2006 *Science* **312** 1322–3
[35] Rossmeisl J, Nørskov J K, Taylor C D, Janik M J and Neurock M 2006 *J. Phys. Chem.* B **110** 21833–9
[36] Skúlason E, Karlberg G S, Rossmeisl J, Bilgaard T, Greeley J, Jónsson H and Nørskov J K 2007 *Phys. Chem. Chem. Phys.* **9** 3241–50
[37] Ogasawara H, Brena B, Nordlund D, Nyberg M, Pelmenschikov A, Petterson L and Nilsson A 2002 *Phys. Rev. Lett.* **89** 276102
[38] Rossmeisl J, Skúlason E, Björketun M E, Tripkovich V and Nørskov J K 2008 *Chem. Phys. Lett.* **466** 68–71
[39] Marcus R 1956 *J. Chem. Phys.* **24** 966
[40] Anderson P W 1961 *Phys. Rev.* **124** 41
[41] Newns M D 1969 *Phys. Rev.* **178** 1123
[42] Santos E, Lundin A, Pötting K, Quaino P and Schmickler W 2009 *Phys. Rev.* B **79** 235436
[43] Coulson C and Danielsson U 1954 *Ark. Fys.* **8** 245–55
[44] Warshel A and Weiss R M 1980 *J. Am. Chem. Soc.* **102** 2523–44
[45] Hwang J-K, King G, Creighton S and Warshel A 1988 *J. Am. Chem. Soc.* **110** 5297–311
[46] Åqvist J and Warshel A 1993 *Chem. Rev.* **93** 2524–44
[47] Lobaugh J and Voth G A 1996 *J. Chem. Phys.* **104** 2056–69
[48] Vuilleumier R and Borgis D 1998 *Chem. Phys. Lett.* **284** 71–7
[49] Sagnella D E and Tuckerman M E 1998 *J. Chem. Phys.* **108** 2073–83
[50] Wilhelm F, Schmickler W, Nazmutdinov R R and Spohr E 2008 *J. Phys. Chem.* C **112** 10814–26
[51] Walbran S and Kornyshev A A 2001 *J. Chem. Phys.* **114** 10039–48
[52] Climent V, Attard G and Feliu J 2002 *J. Electroanal. Chem.* **532** 67
[53] Pajkossy T and Kolb D M 2008 *Electrochim. Acta* **53** 7403
[54] Berendsen H J C, Postma J P M, van Gunsteren W F, DiNola A and Haak J R 1984 *J. Chem. Phys.* **81** 3684–90
[55] Spohr E 1989 *J. Phys. Chem.* **93** 6171
[56] Jacob T and Goddard W A III 2004 *J. Phys. Chem.* B **108** 8311–23
[57] Papoian G, Norskov J and Hoffmann R 2000 *J. Am. Chem. Soc.* **122** 4129–44
[58] Gohda Y, Schnur S and Groß A 2008 *Faraday Discuss.* **140** 233–44
[59] Pecina O and Schmickler W 1997 *J. Electroanal. Chem.* **431** 47–50
[60] Pecina O and Schmickler W 1998 *Chem. Phys.* **228** 265–77